

Adsorptive removal of acid red 88 on cypress-sawdust-based activated carbon by microwave-assisted H_3PO_4 mixed with Fe/Mn/Zn activation

Jin Yuan^a, Lu Yao^{a,b}, Ruzhen Xie^{a,*}, Pengchen Wang^a, Juan Mo^a, Wenju Jiang^{a,b}

^aCollege of Architecture and Environment, Sichuan University, Chengdu 610065, China, Tel. +86-28- 8540 7800, Fax +86-28- 8540 3016, email: 1148240830@qq.com (J. Yuan), yaolu602c@sina.cn (L. Yao), xieruzhen@scu.edu.cn (R.Xie), 1069953121@qq.com (P. Wang), 983792094@qq.com (J. Mo), wenjujiang@scu.edu.cn (W. Jiang)

^bNational Engineering Research Center for Flue Gas Desulfurization, Chengdu 610065, China

Received 29 June 2017; Accepted 7 December 2017

ABSTRACT

In this study, activated carbon was produced from cypress sawdust by microwave-assisted phosphoric acid activation. Three kinds of metal salts ($Fe(NO_3)_3$, $Mn(NO_3)_2$ and $Zn(NO_3)_2$) were used as assisted activating agents to induce carbons' porosity development. The physico-chemical properties of the produced carbons were characterized, the adsorption performance of the produced carbons toward acid red 88 (AR88) were also evaluated. The results showed that with $Fe(NO_3)_3$ assisted activation, the produced carbon (FeAC) showed highest BET surface area ($1758\text{ m}^2\cdot\text{g}^{-1}$) and maximum total pore volume ($1.173\text{ cm}^3\cdot\text{g}^{-1}$), which is 34.0% and 30.9% higher than those without metal salts assisted activation (AC), respectively. While $Mn(NO_3)_2$ assisted activation lead to 53.8% increment of mesopore in MnAC, and resulted highest AR88 adsorptive efficiency. Three isotherm models were used to fit the adsorption data, the maximum adsorption capacity of MnAC was found to be $416.67\text{ mg}\cdot\text{g}^{-1}$ at 298K according to Langmuir model. The kinetics studies showed that chemical process is involved in the AR88 adsorption. The thermodynamic parameters (ΔH^0 , ΔS^0 and ΔG^0) showed that the adsorption process was spontaneous and exothermic. The regeneration of MnAC was also evaluated. The result suggested that metal salts assisted activation can effectively turn cypress sawdust to economic and efficient adsorbents for AR88 removal.

Keywords: Activated carbon; Microwave; Cypress sawdust; Assisted activation; Adsorption; Acid red 88

1. Introduction

The discharge of dye containing industrial effluents has caused increasingly serious problem in recent years due to their adverse effects to many forms of life [1]. Dyes are widely used in various industries such as textile, cosmetics, pharmaceuticals, tannery, printing, paper and food processing [1–4]. Organic dyes especially azo dyes are identified as carcinogenic and mutagenic compounds which are toxic to aquatic organisms and human beings, thus, the treatment of dye containing wastewater is of significant concern [1,2,5]. Different methods including coagulation/flocculation, photocatalytic degradation, electrochemical

oxidation, adsorption and membrane treatment have been applied for the removal of dyes from aqueous solution [6–8]. Among these technologies, adsorption onto activated carbon has been recognized as the most promising method due to its high efficiency and easy operation [8,9]. However, the high cost of activated carbon restricted its wide application.

In order to reduce the carbon cost, researchers have come up with abundant low cost precursor to produce activated carbon, such as agricultural and industrial waste, including sawdust, plum stones, rice hull and waste tires [10–13]. These carbonaceous precursor can be turned to activated carbon by physical or chemical activation in the temperatures ranging from 500 to 1000°C.

*Corresponding author.

Conventional electrical furnace heating is the most common used heating method to obtain activated carbon. However, it has many drawbacks such as the non-uniform heat distribution in the furnace and the necessity of long time pyrolysis in high temperature [14]. Microwave irradiation is based on dielectric heating, pyrolysis by microwave heating has many advantages over conventional electrical furnace heating, such as uniform interior and volumetric heating, high heating rate, short treatment time, and easy scale up [15,16]. Recently, it was found that metals and metal oxides can be used as trigger for plasma under microwave irradiation, which could enhance the adsorption of microwave energy and greatly promote the process and effectiveness of electromagnetic energy converting to thermal energy [13,17,18]. Besides, many researchers reported that metal salts such as Fe^{3+} , Mn^{2+} and Zn^{2+} can be used as catalyst to change the surface chemistry of the produced carbons [19–21]. Thus, we propose to produce activated carbon using different metal salts as assisted activator in microwave-assisted H_3PO_4 activation process. In this process, metal salts could act as catalysis hotspot under microwave irradiation which could save energy, and metal salts could also induce carbon porosity development and surface chemistry modification during carbon activation process.

In this study, cypress sawdust, a waste from furniture manufacturing, was used as raw material, three kinds of metal salts ($\text{Fe}(\text{NO}_3)_3 \cdot 9\text{H}_2\text{O}$, $\text{Mn}(\text{NO}_3)_2$ and $\text{Zn}(\text{NO}_3)_2 \cdot 6\text{H}_2\text{O}$) were used as assisted activating agents to prepare activated carbon (AC) under microwave irradiation. The physical and chemical properties of the produced carbons (ACs) were characterized by SEM, XRD, FTIR and XPS. The adsorption capacities of the ACs were attempted for AR88 removal from aqueous solution. The adsorption equilibrium, kinetics and thermodynamic were analyzed to study the mechanism of acid red 88 (AR88) removal by the produced ACs.

2. Materials and methods

2.1. Materials and activated carbon preparation

Cypress sawdust was obtained from Sichuan province, China. The main chemical composition of cypress sawdust was (wt. %): C, 43.10%; H, 5.31%; O, 51.35%; S, 0.13%; N, 0.11%. All chemical reagents were of analytical grade.

Raw cypress sawdust was grinded, sieved and dried before use. The preparation method was similar to our former report [22]. H_3PO_4 , cypress sawdust and M^{n+} was mixed in a weight ratio of 1.94:100:3 (M^{n+} refers to Fe^{3+} in $\text{Fe}(\text{NO}_3)_3 \cdot 9\text{H}_2\text{O}$, Mn^{2+} in $\text{Mn}(\text{NO}_3)_2$ and Zn^{2+} in $\text{Zn}(\text{NO}_3)_2 \cdot 6\text{H}_2\text{O}$). The mixtures were agitated and then immersed for 24 h under room temperature. After that, the slurry was calcined at 475 W for 8 min and 50 s under nitrogen atmosphere in a microwave oven. After cooling in N_2 , the sample was boiled with "1+9" HCl for 30 min to remove impurities, and then washed thoroughly with hot deionized water until the pH of filtrate was constant. The resulting carbon was dried, crushed and sieved to pass through a 200-mesh screen. The produced carbons were named AC, FeAC, MnAC and ZnAC, respectively.

2.2. Adsorption experiment

Batch adsorption experiments were conducted in a rotary shaker at 298–318 K by agitating certain amount of ACs in 50 mL AR88 with desired concentration and initial solution pH values at 180 rpm for 3 h to reach equilibrium. After that, the samples were filtered and the residual AR88 concentration was analyzed by UV-vis spectrometer at 506 nm. All experiments were performed in triplicate and the mean values were presented.

2.3. Adsorption models

Three kinetic models, Pseudo-first-order, Pseudo-second-order and Intra-particle diffusion models were employed to fit the experimental data to investigate the possible adsorption mechanism towards AR88. The equations are expressed as follows [2,23]:

$$\ln(q_e - q_t) = \ln q_e - k_1 t \quad \text{Pseudo-first-order} \quad (1)$$

$$\frac{t}{q_t} = \frac{1}{k_2 \times q_e^2} + \frac{t}{q_e} \quad \text{Pseudo-second-order} \quad (2)$$

$$q_t = k_{pi} t^{0.5} + C_i \quad \text{Intra-particle diffusion} \quad (3)$$

where q_e and q_t ($\text{mg} \cdot \text{g}^{-1}$) are the adsorption capacities of ACs at equilibrium and time t (min), respectively. k_1 ($\text{mg}(\text{g} \cdot \text{min})^{-1}$) is the pseudo-first-order rate constant, k_2 ($\text{g}(\text{mg} \cdot \text{min})^{-1}$) is the pseudo-second-order rate constant, k_{pi} ($\text{mg}(\text{g} \cdot \text{min}^{1/2})^{-1}$) is the intra-particle diffusion rate constant, and C_i is the intercept presenting the thickness of boundary layer.

In order to clarify the interaction relation between the ACs and AR88 at constant temperature, the adsorption equilibrium data were fitted with Langmuir model ($C_e/q_e = 1/KQ_m + C_e/Q_m$, (4)), Freundlich model ($q_e = k_f C_e^{1/n}$, (5)) and Temkin model ($q_e = B \ln K_T + B \ln C_e$, (6)), where $B = RT/b$. The Langmuir constant Q_m ($\text{mg} \cdot \text{g}^{-1}$) is the maximum adsorption amount, K ($\text{L} \cdot \text{mg}^{-1}$) is the Langmuir isotherm constant, C_e ($\text{mg} \cdot \text{L}^{-1}$) is the AR88 concentration at equilibrium, q_e ($\text{mg} \cdot \text{g}^{-1}$) is the amount of AR88 adsorbed onto ACs under equilibrium. The Freundlich isotherm constant K_f ($\text{mg}(\text{L}/\text{mg})^{1/n}$) and n indicate the adsorption capacity and intensity, respectively. K_T ($\text{L} \cdot \text{mg}^{-1}$) and b are the Temkin constants, T is the absolute temperature (K), and R is the universal gas constant ($8.314 \text{ J}(\text{mol} \cdot \text{K})^{-1}$) [24,25].

To investigate the nature of the process for AR88 adsorption onto ACs, the thermodynamic parameters such as changes in enthalpy (ΔH^0), entropy (ΔS^0) and free energy (ΔG^0) were calculated using the equations as follows [2,26]:

$$\ln k_d = \frac{\Delta S^0}{R} - \frac{\Delta H^0}{RT} \quad (4)$$

$$\Delta G^0 = -RT \ln k_d \quad (5)$$

In which, k_d is the distribution coefficient, ΔS^0 ($\text{J}(\text{mol} \cdot \text{K})^{-1}$) is standard entropy; ΔH^0 ($\text{kJ}(\text{mol} \cdot \text{K})^{-1}$) is standard enthalpy, R ($8.314 \text{ J}(\text{mol} \cdot \text{K})^{-1}$) is the gas constant and T (K) the absolute temperature.

2.4. Regeneration experiments

The efficiency of regeneration was carried out using five consecutive adsorption-desorption cycles. For adsorption cycle, the $\text{Mn}(\text{NO}_3)_2$ assisted activated carbons (MnAC) were reacted 3 h in 50 mL $250 \text{ mg}\cdot\text{L}^{-1}$ AR88 solution at 298 K to reach equilibrium. After that, the AR88-loaded carbons were washed with deionized water (1000 mL DI/(gMnAC)) to remove AR88. The exhausted carbons were dried overnight at 378 K and microwave regenerated at 300 W for 5 min under nitrogen atmosphere.

2.5. Characterization of activated carbon

The surface morphology of activated carbons was identified by SEM (JEOL, JSM-7500 F, Japan). The BET surface area and porosity of the produced carbons were determined from N_2 adsorption-desorption isotherms at 77 K using the surface area analyzer (SAP 2460, Micromeritics, USA). The crystallography of the produced carbons was confirmed using XRD (X-Pert PRO MPD, Panalytical, NL) with Cu K α as the radiation source with 2θ range of 10–80°. The surface groups of activated carbons were studied by FTIR spectrometer at a resolution of 4 cm^{-1} (Tensor 27 spectrometer, FTIR-6700, Nicolet,

USA). The surface elemental compositions on the produced carbons were characterized using XPS (XSAM-800, KRATOS, UK), the binding energies were calibrated based on C 1s peak at 284.6 eV. The surface charge of the produced carbons was evaluated according to its point of zero charge (pH_{PZC}) using the method proposed by Reddy et al. [3].

3. Results and discussion

3.1. Physico-chemical properties

From SEM images of the produced carbons in Fig. 1, a large amount of cavities and pores with different shapes on the ACs can be observed, which might result from the evaporation of H_3PO_4 during carbonization [27], thus leaving the space previously occupied.

The yield and porous structure parameters of ACs are listed in Table 1. It could be seen that by assisted activation with metal salts ($\text{Fe}(\text{NO}_3)_3$, $\text{Mn}(\text{NO}_3)_2$ and $\text{Zn}(\text{NO}_3)_2$), the BET surface area and pore volume of the carbons increased dramatically. The BET surface area and total pore volume of the resulted carbons was in the order: FeAC > MnAC > ZnAC > AC. Assisted activation with Fe^{3+} resulted in high-

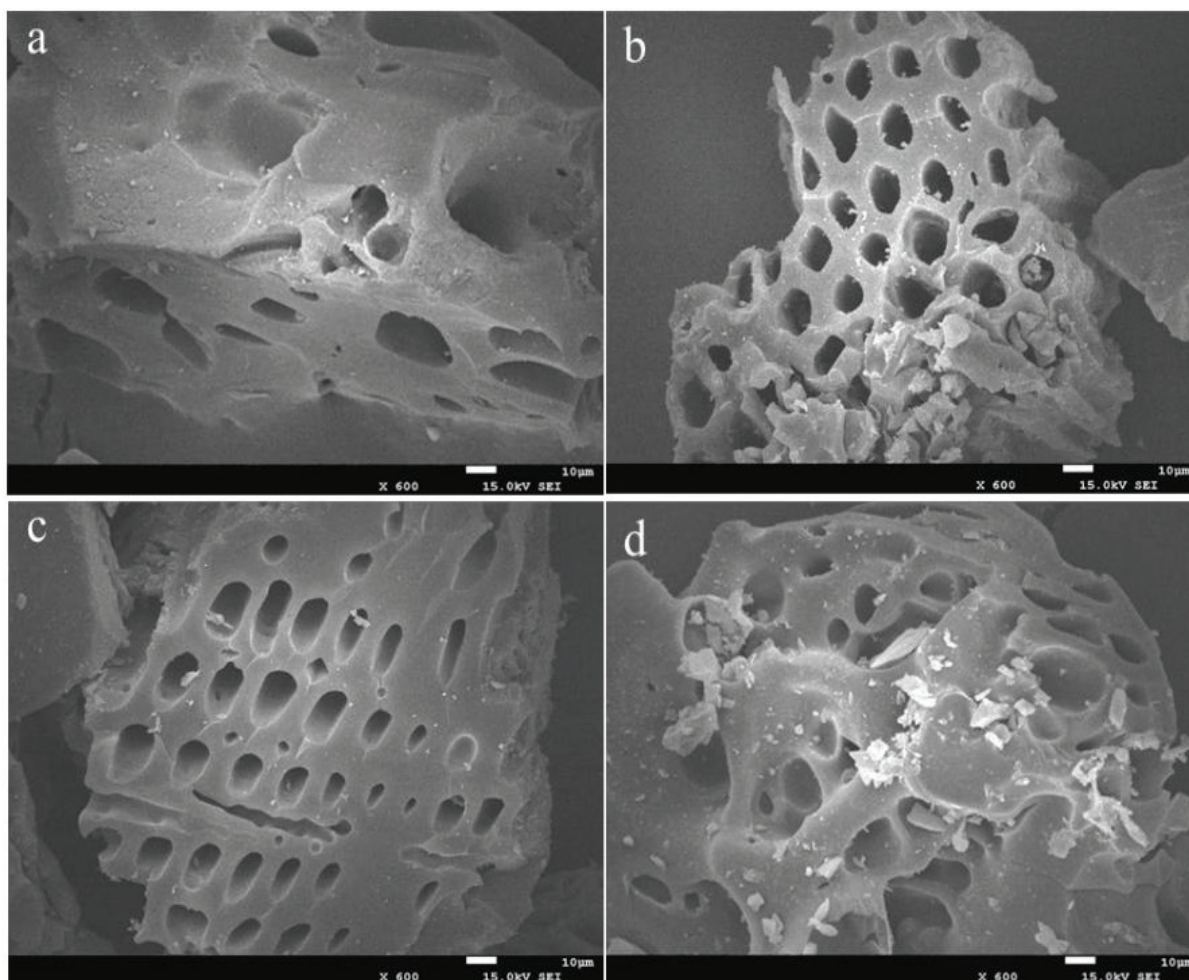


Fig. 1. SEM of AC (a), FeAC (b), MnAC (c) and ZnAC (d).

Table 1
The yield and textural properties of the produced carbons

| Carbon | SBET (m ² ·g ⁻¹) | Smic (m ² ·g ⁻¹) | Sest (m ² ·g ⁻¹) | Vtot (cm ³ ·g ⁻¹) | Vmic (cm ³ ·g ⁻¹) | Vmes (cm ³ ·g ⁻¹) | Vmac (cm ³ ·g ⁻¹) | Dp (nm) | Yield (%) | pHpzc |
|--------|--|--|--|---|---|---|---|------------|--------------|-------|
| AC | 1312 | 196 | 1116 | 0.895 | 0.069 | 0.532 | 0.294 | 3.33 | 42.57 | 2.59 |
| FeAC | 1758 | 182 | 1576 | 1.173 | 0.075 | 0.770 | 0.328 | 3.32 | 43.01 | 2.67 |
| MnAC | 1659 | 140 | 1519 | 1.161 | 0.052 | 0.819 | 0.290 | 3.43 | 43.39 | 2.75 |
| ZnAC | 1338 | 163 | 1175 | 0.912 | 0.071 | 0.592 | 0.249 | 3.43 | 43.43 | 2.84 |

est BET surface and largest pore volume, which is 34.0% and 30.9% higher than those of AC without metal salt addition. The introduction of Zn²⁺ is favorable for mesoporous volume development and resulted in 11.2% increment in mesopores compared with that of AC. Addition of Mn²⁺ lead to a increment in BET surface area and pore volume, although not as high as that of Fe³⁺ modified one. It is worth to notice that, Mn²⁺ modified AC showed the largest mesoporous volume (0.819 cm³·g⁻¹), which is 53.8% higher than that of AC. These results suggested the introduction of metal salt could induce the pore structure development on ACs. Fe³⁺ could act as catalysis hotspot for micropore, mesopore and macropore development on ACs when mixing with H₃PO₄, and Mn²⁺ could largely induce mesopore development under microwave irradiation. For the highly development of mesopore in MnAC, fast mass transfer channel was available in MnAC for large molecular adsorption. Besides, it can be seen from Table 1 that the addition of metal salts did not significantly affect the yield of ACs.

Fig. 2 shows the XRD patterns of the four ACs. A broad diffraction peak at around 24.8° and a weak diffraction peak at 44.5° corresponding to 002 and 100 graphite-like reflections, respectively, were observed in the XRD patterns of all ACs. This feature revealed that both the AC and metal salt modified AC have turbostratic structures [28]. AC without metal salts activation showed relatively a more definite peak at 44.5°. This was related to the decrease in the microcrystallite zones of graphite in the ACs as the addition of metal salts [29]. No obvious new diffraction peaks were observed after the introduction of Fe, Mn and Zn, which indicated the metal salts might in an amorphous phase after HCl washing.

XPS analysis was carried out to further clarify the chemical forms of surface elements on the ACs. The wide scan spectra of AC, MnAC and MnAC after adsorbing AR88 are shown in Fig. 3. The low peak of Mn 2p indicated slightly left of manganese on MnAC during Mn(NO₃)₂ activation after HCl washing. From XPS analysis result, with Mn addition, the oxygen content increased from 10.72% to 13.28%, which indicates oxygen containing functional groups were introduced by Mn addition during carbon activation. C 1s and O 1s XPS corresponding binding energy and relative content are listed in Table 2. The C 1s peaks of AC and MnAC can be deconvoluted into four peaks, including C–C (BE = 284.6–284.7 eV), C–O (BE = 285.9–286.1 eV), C=O (BE = 287.4–288.3 eV) and O=C–OH (BE = 289.7–290.0 eV) [30–32]. As can be seen from Table 2, the relative content of C=O and O=C–OH in MnAC were 9.17% and 6.55%, respectively, which were higher than those in AC, i.e., the content of C=O and O=C–OH in AC were only 6.55% and 2.38%, respectively. Thus, it indicated that the introduction of Mn lead to

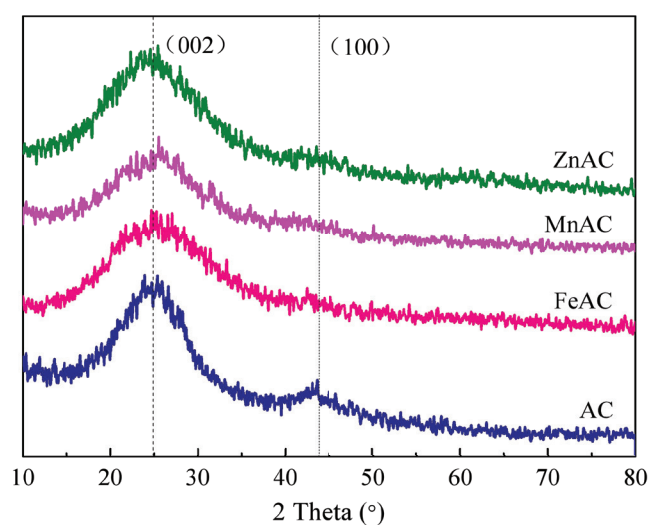


Fig. 2. XRD patterns of the produced ACs.

the increment of the surface oxygen containing functional groups on AC. It is interesting to note that, after adsorbing AR88, the relative content of O=C–OH decreased obviously, which suggested that, during the adsorption process, the O=C–OH in MnAC might react with AR88.

IR spectra of MnAC before and after AR88 adsorption are shown in Fig. 4. FTIR spectra confirmed the presence of multiple functional groups on ACs. The absorption bands at 3430 and 3320 cm⁻¹ can be assigned to the stretching vibration of hydroxyl groups (O–H) on the surface of activated carbons. After activation by Mn(NO₃)₂, the peak between 2920 and 2850 cm⁻¹ of bond stretching O–H in methyl and methylene groups was observed on MnAC [33,34], which indicated that the oxygen containing functional groups were introduced by Mn addition during carbon activation. The peaks located at 1694 and 1682 cm⁻¹ can be characterized as carbonyl group stretching from carboxyl, the peaks at 1613, 1570 and 1559 cm⁻¹ are the signal of the stretch vibration in aromatic rings [35,36]. The transmittance at 1155 cm⁻¹ is identical to C–O [36]. After adsorption of AR88, a clearly new peak appeared in 1037 cm⁻¹, which may be assigned to C–N stretching vibrations from the adsorbed AR88 molecules [37]. Also, the position of the peaks relating to carbonyl group in carboxyl changed after AR88 adsorption, suggesting the involvement of hydroxyl groups in AR88 uptake, this result is in accordance with the XPS analysis.

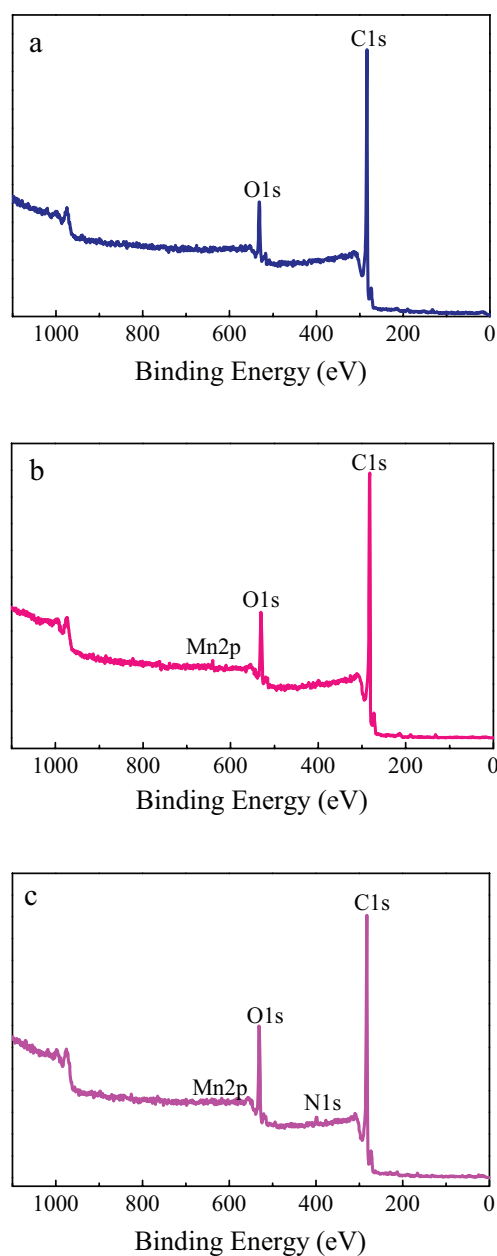


Fig.3. XPS spectra of wide scan spectra for (a) AC, (b) MnAC and (c) AR88-loaded MnAC.

3.2. Effect of carbon dose

The effect of carbon dosages on AR88 removal was studied by varying ACs amount from 0.4 to 2 g·L⁻¹, the results are shown in Fig. 5. As can be seen from Fig. 5, the removal rate of AR88 increased rapidly with the increment of ACs' amount. By increasing dosage, more adsorption sites were available for a certain amount of AR88, and the diffusion of AR88 molecules onto activated carbons surface became easier, thus higher removal rate was achieved. It can also be observed in Fig. 5, with metal salts assisted activation, ACs exhibited better adsorption capacity, with the order of MnAC > FeAC > ZnAC > AC, revealing that activation with metal salts can significantly improve ACs' adsorption capacity toward AR88. This is related to the catalytic effect of metal salts on the carbon porosity development and surface groups on samples. Among the ACs, MnAC exhibited highest AR88 removal capacity, with dosage of 0.8 g·L⁻¹ achieved 100% AR 88 removal, which is almost 3 times higher than that of AC, this could due to higher mesopore volume in MnAC, thus allowed better diffusion of the large sized AR88 molecules into the inner matrix and also provide more active sites for AR88 adsorption [38].

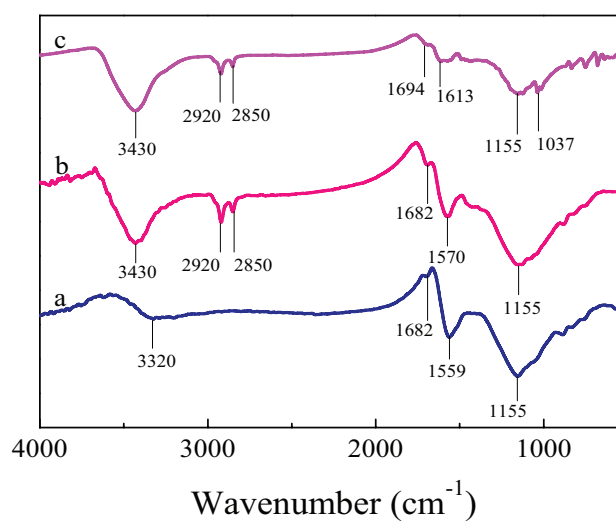


Fig. 4. IR spectra of AC (a), MnAC (b) and AR88-loaded MnAC (c).

Table 2

The binding energy (BE) and relative content (RC) of C 1s and O 1s for AC and MnAC

| Samples | AC | | MnAC | | MnAC after AR88 adsorption | | |
|---------|------------|--------|---------|--------|----------------------------|--------|-------|
| | BE (eV) | RC (%) | BE (eV) | RC (%) | BE (eV) | RC (%) | |
| C1s | C–C | 284.7 | 68.87 | 284.6 | 65.72 | 284.6 | 63.75 |
| | C–O | 286.1 | 22.20 | 285.9 | 18.60 | 285.9 | 28.05 |
| | C=O | 288.3 | 6.55 | 287.5 | 9.17 | 287.5 | 5.30 |
| | O=C–OH | 289.9 | 2.38 | 289.7 | 6.51 | 289.8 | 2.90 |
| O1s | oxides | 530.9 | 26.83 | 531.3 | 28.65 | 531.4 | 26.85 |
| | C–O or C=O | 532.5 | 52.05 | 532.9 | 47.69 | 532.9 | 55.46 |
| | –OH | 533.7 | 21.12 | 534.3 | 23.66 | 534.2 | 17.69 |

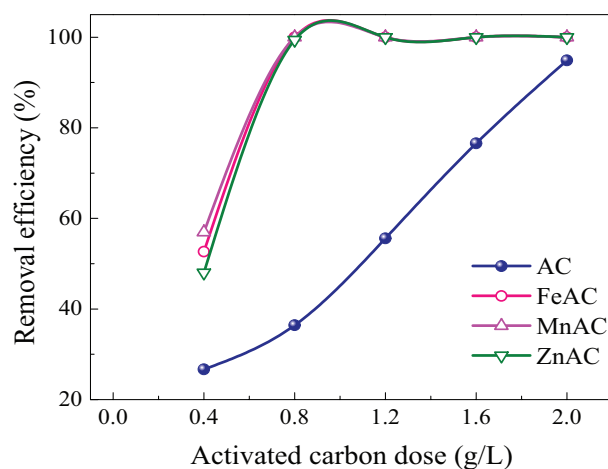


Fig. 5. The influence of ACs dose on the adsorption of AR88 ($C_{\text{AR88}} = 250 \text{ mg}\cdot\text{L}^{-1}$; contact time 3 h; initial solution pH = 7.58; temperature 298 K).

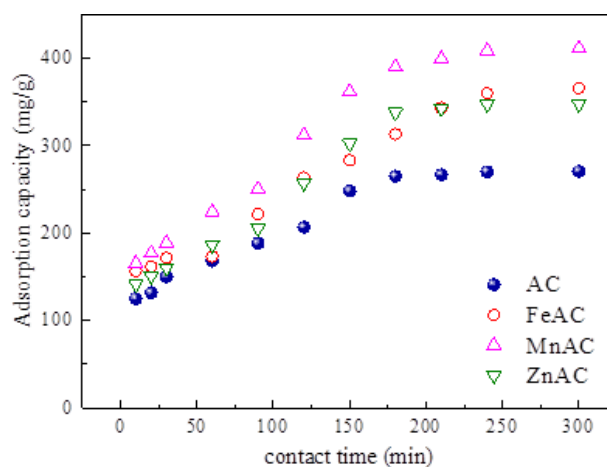


Fig. 7. Effect of agitation time on AR88 adsorption onto carbons ($C_{\text{AR88}} = 250 \text{ mg}\cdot\text{L}^{-1}$; carbon dosage = $0.4 \text{ g}\cdot\text{L}^{-1}$; initial solution pH = 5.0; temperature 298 K).

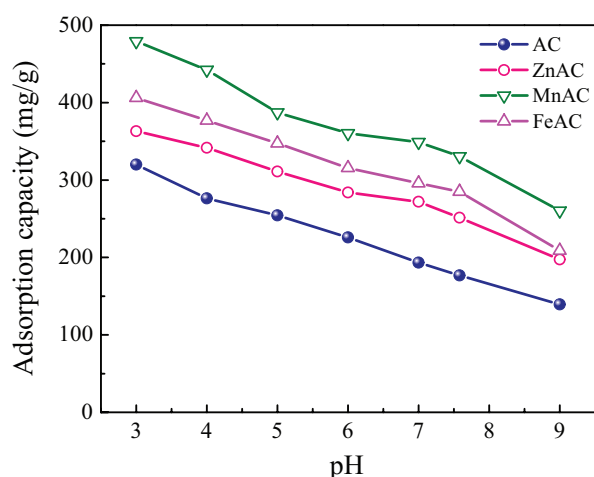


Fig. 6. Adsorption capacity of AR88 in aqueous solution as a function of pH ($C_{\text{AR88}} = 250 \text{ mg}\cdot\text{L}^{-1}$; contact time = 3 h; dosage = $0.4 \text{ g}\cdot\text{L}^{-1}$; temperature 298 K).

3.3. Effect of pH

The adsorption of AR88 onto the four ACs was significantly influenced by initial solution pH (Fig. 6). The adsorption capacity of AR88 decreased with the increase of initial solution pH. As can be seen from Table 1, the pH_{pzc} of ACs are 2.59, 2.67, 2.75 and 2.84 for AC, FeAC, MnAC and ZnAC, respectively. At $\text{pH} > \text{pH}_{\text{pzc}}$, the ACs' surface are negatively charged, while AR88 is an anionic mono azo dye [2]. By increasing pH, the ACs' surface became increasing negatively charged, thus the electrostatic repulsion between the negatively charged adsorption sites and negatively charged AR88 anions increased and lead to a decrease in AR88 adsorption capacity.

3.4. Adsorption kinetics

Fig. 7 shows the removal of AR88 by the produced ACs as a function of reaction time. For all ACs, the removal rate

increased very fast at initial stage and gradually slowed down with further interaction time. Finally, equilibrium was achieved after interaction time of 250 min. Thus, 300 min was chose in further experiments. In order to study mechanism of AR88 adsorption process, pseudo-first-order model and pseudo-second-order model were employed to fit the experimental data (Table 3). The results showed the adsorption of AR88 onto ACs follows pseudo-second-order model, suggesting that the chemical process might be the rate-limiting step controlling the adsorption process [2].

Adsorption kinetics was further investigated using intra-particle diffusion model to study the steps of diffusion mechanism. As can be seen from Table 3, for all ACs, the plot of q_t versus $t^{1/2}$ are multilinear and did not pass through the origin, indicating the intra-particle diffusion was not the unique rate-controlling step, other processes (such as external mass transfer, surface diffusion or chemical reaction) might involve in the adsorption process [39].

3.5. Adsorption isotherms

The adsorption isotherms were fitted to Langmuir, Freundlich and Temkin adsorption models. The isotherm constants are reported in Table 4. From Table 4, it can be seen that the correlation coefficient (R^2) of the three isotherms followed the order: Langmuir > Temkin > Freundlich. Langmuir isotherm fitted best to the adsorption data, suggesting the homogeneous nature of four ACs [1]. The maximum adsorption capacity towards AR88 calculated from Langmuir isotherm was 322.58, 408.16, 416.67 and 370.37 $\text{mg}\cdot\text{g}^{-1}$, for AC, FeAC, MnAC and ZnAC at 298 K, respectively. The adsorption capacity follows the order: MnAC > FeAC > ZnAC > AC, which was in the same order of the ACs' mesopore volume development as shown in Table 1.

The positive value of Tempkin constant B indicates adsorption of AR88 onto ACs is an exothermic process [40]. This case is in accordance with the experimental phenomenon: the adsorption capacity of AR88 decreased with the increase of temperature. The value of Freundlich constant n was higher than 1, indicating a favorable process.

Table 3

Kinetics constants for AR88 adsorption on ACs ($C_{AR88} = 250 \text{ mg}\cdot\text{L}^{-1}$; carbon dosage = $0.4 \text{ g}\cdot\text{L}^{-1}$; initial solution pH = 5.0; temperature 298 K)

| Kinetic models | Parameters | Carbons | | | |
|-------------------------------------|---|---------|---------|---------|---------|
| | | AC | AC-Fe | AC-Mn | AC-Zn |
| Pseudo-first-order parameters | $q_{e,exp}$ (mg/g) | 270.92 | 365.92 | 411.46 | 347.54 |
| | $q_{e,cal}$ (mg/g) | 309.76 | 352.41 | 477.80 | 1112.43 |
| | K_1 (min^{-1}) | 0.021 | 0.013 | 0.018 | 0.035 |
| | R^2 | 0.8991 | 0.8470 | 0.8990 | 0.6431 |
| Pseudo-second-order parameters | $q_{e,cal}$ (mg/g) | 303.03 | 416.67 | 476.19 | 400.00 |
| | K_2 ($\text{g}/(\text{mg}\cdot\text{min})$) | 0.00010 | 0.00005 | 0.00004 | 0.00005 |
| | R^2 | 0.9824 | 0.9538 | 0.9695 | 0.9602 |
| Intra-particle diffusion parameters | K_p ($\text{mg}/\text{g}\cdot\text{min}^{0.5}$) | 12.097 | 17.120 | 20.732 | 17.665 |
| | C | 82.759 | 78.155 | 83.752 | 69.335 |
| | R^2 | 0.9559 | 0.9547 | 0.9577 | 0.9444 |

Table 4

Isotherm parameters for the AR88 adsorption onto carbons ($C_{AR88} = 100\text{--}300 \text{ mg}\cdot\text{L}^{-1}$; contact time = 3 h; carbon dosage = $0.4 \text{ g}\cdot\text{L}^{-1}$; initial solution pH = 5.0)

| Isotherms | Parameters | Temperature | | | | | |
|------------|--|-------------|--------|--------|--------|--------|--------|
| | | 298 K | | 308 K | | 318 K | |
| Langmuir | Carbons | AC | FeAC | MnAC | ZnAC | MnAC | MnAC |
| | $Q_{m,cal}$ (mg/g) | 322.58 | 408.16 | 416.67 | 370.37 | 285.71 | 212.77 |
| | K_L (L/mg) | 0.054 | 0.048 | 0.073 | 0.054 | 0.040 | 0.015 |
| Freundlich | R^2 | 0.9978 | 0.9823 | 0.9895 | 0.9823 | 0.9785 | 0.9908 |
| | K_F ($\text{mg}/\text{g}(\text{L}/\text{mg})^{1/n}$) | 88.69 | 73.27 | 99.23 | 74.47 | 52.81 | 21.87 |
| | n | 4.18 | 3.01 | 3.49 | 3.21 | 3.25 | 2.65 |
| Temkin | R^2 | 0.8828 | 0.8218 | 0.8277 | 0.7749 | 0.7386 | 0.9764 |
| | K_T (L/mg) | 1.181 | 0.441 | 0.877 | 0.514 | 0.396 | 0.133 |
| | B | 28.4 | 27.64 | 29.89 | 31.02 | 42.51 | 53.92 |
| | R^2 | 0.9139 | 0.8476 | 0.8625 | 0.7862 | 0.7662 | 0.9540 |

3.6. Thermodynamic parameters

Adsorption experiments were conducted at 298–318 K to investigate the effect of temperature, with initial AR88 concentration of $100 \text{ mg}\cdot\text{L}^{-1}$, MnAC of $0.4 \text{ g}\cdot\text{L}^{-1}$ at initial pH = 5.0. The thermodynamic parameters (ΔH^0 , ΔG^0 and ΔS^0) for AR88 adsorption onto MnAC is shown in Table 5. The negative value of ΔH^0 ($-67.47 \text{ kJ}(\text{mol}\cdot\text{K})^{-1}$) indicates that adsorption of AR88 onto MnAC is an exothermic process, which is in accordance with the result of isotherm investigation. The negative values of ΔG^0 (-3.71 , -0.86 and $-0.11 \text{ kJ}\cdot\text{mol}^{-1}$) at all temperatures indicate the adsorption of AR88 onto MnAC was spontaneous and thermodynamically favorable [41]. The increase in ΔG^0 with temperature increased from 298 to 318 K suggesting that adsorption favorable at lower temperatures. The negative value of ΔS^0 ($-219.00 \text{ J}(\text{mol}\cdot\text{K})^{-1}$) indicates a decrease in the degree of freedom during AR88 adsorption onto MnAC [26].

3.7. Microwave regeneration

The results of MnAC adsorption capacity as a function of regeneration cycles are shown in Fig. 8. From Fig. 8, it can

Table 5

Thermodynamic parameters for AR88 adsorption onto MnAC at different temperatures

| Temperature (K) | K_d | ΔG^0 ($\text{kJ}\cdot\text{mol}^{-1}$) | ΔS^0 ($\text{J}(\text{mol}\cdot\text{K})^{-1}$) | ΔH^0 ($\text{kJ}(\text{mol}\cdot\text{K})^{-1}$) |
|-----------------|-------|--|---|--|
| 298 | 4.47 | -3.71 | | |
| 308 | 1.4 | -0.86 | -219 | -67.47 |
| 318 | 1.04 | -0.11 | | |

be seen that the MnAC lost 32.0% of its adsorption capacity after the first two cycles, after that, the adsorption capacity slightly reduced from the third to fifth cycle, adsorption capacity remained $201.14 \text{ mg}\cdot\text{g}^{-1}$ after five recycles, which is still higher than that of many other adsorbent as shown in Table 6. The loss of adsorption capacity might due to the partial collapse of porosity in MnAC because of thermal heating, which lead to large amount of gases releasing and internal reorganization of carbon structure, and also may due to the incomplete desorption of AR88 molecules which lead to pore blockage.

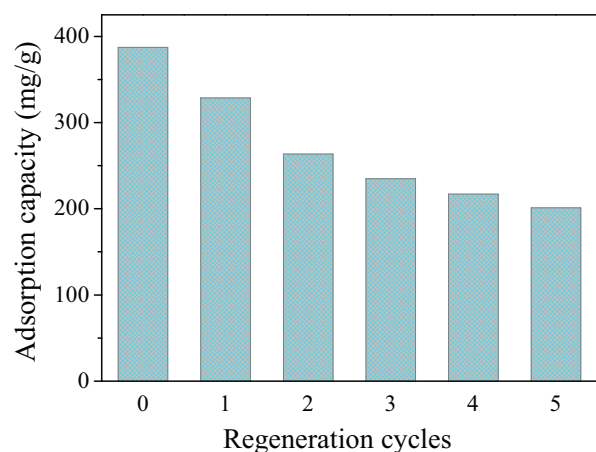


Fig. 8. The adsorption capacity of MnAC in five adsorption-regeneration experiments.

3.8. Adsorption mechanism

Based on the experimental and characterization studies, the adsorption of AR88 by the prepared ACs may be ascribed to physical adsorption, and chemical interaction between the AR88 molecules and the surface groups on ACs. The adsorption capacity follows the order: MnAC > FeAC > ZnAC > AC, which was in the same order of the ACs' mesopore volume development as shown in Table 1. The development of mesopore in ACs plays an important role in AR88 physical adsorption onto ACs, while the micropore seem to be of less importance for AR88 removal, for mesopore would provide fast mass transfer channel and more active sites for large molecular adsorption. The presence of functional groups especially hydroxyl group on carbons surface can enhance AR88 uptake.

Table 6 summarizes a comparative adsorption capacity of different adsorbents for AR88 removal. As can be observed in Table 6, cypress-sawdust-based ACs in this study showed higher adsorption capacity toward AR88 compared with other adsorbents, which indicates microwave-induced metal salts mixing phosphoric acid activation is an effective way to turn cypress sawdust into effective adsorbent, the cheap metal salts would act as catalysis hotspot under microwave irradiation, which would induce carbon porosity development, and enhance carbon adsorptive capacity toward AR88.

4. Conclusions

Results showed metal salts could act as catalysis hotspot for carbon porosity development under microwave irradiation. The BET surface area and the total pore volume of the produced carbon followed the order: FeAC > MnAC > ZnAC > AC. Activation with $Mn(NO_3)_2$ resulted highest mesopore volumes and best AR88 removal capacity (maximum monolayer adsorption capacity of 416.67 $mg \cdot g^{-1}$ at 298 K). The adsorption capacities of AR88 followed the order of MnAC > FeAC > ZnAC > AC, which is in the same order of carbon's mesopore development. The equilibrium adsorption of AR88 on all ACs fitted Langmuir isotherms. The adsorption

Table 6

The comparison of maximum monolayer adsorption of AR88 onto various adsorbents

| Adsorbent | Adsorption capacity ($mg \cdot g^{-1}$) | References |
|-----------------------------------|---|------------|
| AC | 322.58 | This study |
| FeAC | 408.16 | This study |
| MnAC | 416.67 | This study |
| ZnAC | 370.37 | This study |
| Azolla filiculoides | 123.50 | [4] |
| Bio-silica/chitosan nanocomposite | 25.84 | [41] |
| Azolla rongpong | 78.74 | [42] |
| Azolla microphylla | 54.89 | [43] |
| Anion exchange membrane | 227.1 | [44] |

kinetic can be well described by Pseudo-second order model. The adsorption of AR88 onto ACs is a spontaneous and exothermic process. The regeneration studies revealed the reusability of the produced carbon. These results illustrate the effectiveness of using metal salts as assisted activator in microwave-assisted phosphoric acid activation to prepare activated carbon, and the resulted cypress sawdust-based carbon has great potential for AR88 removal.

Acknowledgment

The authors acknowledge the funding support from the Sichuan Province Science and technology department (China, grant No. 2017HH0065). The author also thank the support from Education Department of Sichuan Province (China, grant No. 17ZA0240) and Chengdu Science and Technology Department (grant No. 2016-HM01-00069-SF).

References

- [1] Z. Noorimotlagh, R. Darvishi Cheshmeh Soltani, A.R. Kha-tae, S. Shahriyar, H. Nourmoradi, Adsorption of a textile dye in aqueous phase using mesoporous activated carbon prepared from Iranian milk vetch, *J. Taiwan Inst. Chem. Eng.*, 45 (2014) 1783–1791.
- [2] F. Bouaziz, M. Koubaa, F. Kallel, F. Chaari, D. Driss, R.E. Ghorbel, S.E. Chaabouni, Efficiency of almond gum as a low-cost adsorbent for methylene blue dye removal from aqueous solutions, *Ind. Crop. Prod.*, 74 (2015) 903–911.
- [3] P.M.K. Reddy, P. Verma, C. Subrahmanyam, Bio-waste derived adsorbent material for methylene blue adsorption, *J. Taiwan Inst. Chem. Eng.*, 58 (2016) 500–508.
- [4] T.V. Padmesh, K. Vijayaraghavan, G. Sekaran, M. Velan, Batch and column studies on biosorption of acid dyes on fresh water macro alga *Azolla filiculoides*, *J. Hazard. Mater.*, 125 (2005) 121–129.
- [5] M. Roushani, Z. Saedi, T. Musa beygi, Anionic dyes removal from aqueous solution using TMU-16 and TMU-16-NH₂ as isorecticular nanoporous metal organic frameworks, *J. Taiwan Inst. Chem. Eng.*, 66 (2016) 164–171.
- [6] A.H. Jawad, R.A. Rashid, M.A.M. Ishak, L.D. Wilson, Adsorption of methylene blue onto activated carbon developed from biomass waste by H₂SO₄ activation: kinetic, equilibrium and thermodynamic studies, *Desal. Water Treat.*, 57 (2016) 25194–25206.

- [7] A. dos Santos, M.F. Viante, P.P. dos Anjos, N. Naidek, M.P. Moises, E.G. de Castro, A.J. Downs, C.A.P. Almeida, Removal of astrazon blue dye from aqueous media by a low-cost adsorbent from coal mining, *Desal. Water Treat.*, 57 (2016) 27213–27225.
- [8] E. Daneshvar, M.S. Sohrabi, M. Kousha, A. Bhatnagar, B. Aliakbarian, A. Converti, A.-C. Norrström, Shrimp shell as an efficient bioadsorbent for Acid Blue 25 dye removal from aqueous solution, *J. Taiwan Inst. Chem. Eng.*, 45 (2014) 2926–2934.
- [9] M.M. Góes, M. Keller, V. Masiero Oliveira, L.D.G. Villalobos, J.C.G. Moraes, G.M. Carvalho, Polyurethane foams synthesized from cellulose-based wastes: Kinetics studies of dye adsorption, *Ind. Crop. Prod.*, 85 (2016) 149–158.
- [10] J. Kazmierczak-Razna, B. Gralak-Podemska, P. Nowicki, R. Pietrzak, The use of microwave radiation for obtaining activated carbons from sawdust and their potential application in removal of NO₂ and H₂S, *Chem. Eng. J.*, 269 (2015) 352–358.
- [11] P. Nowicki, H. Wachowska, R. Pietrzak, Active carbons prepared by chemical activation of plum stones and their application in removal of NO₂, *J. Hazard. Mater.*, 181 (2010) 1088–1094.
- [12] M. Hofman, R. Pietrzak, Adsorbents obtained from waste tires for NO₂ removal under dry conditions at room temperature, *Chem. Eng. J.*, 170 (2011) 202–208.
- [13] S. Lv, X. Chen, Y. Ye, S. Yin, J. Cheng, M. Xia, Rice hull/MnFe₂O₄ composite: Preparation, characterization and its rapid microwave-assisted COD removal for organic wastewater, *J. Hazard. Mater.*, 171 (2009) 634–639.
- [14] J. Kazmierczak-Razna, P. Nowicki, R. Pietrzak, The use of microwave radiation for obtaining activated carbons enriched in nitrogen, *Powder Technol.*, 273 (2015) 71–75.
- [15] D.A. Jones, T.P. Lelyveld, S.D. Mavrofidis, S.W. Kingman, N.J. Miles, Microwave heating applications in environmental engineering—a review, *Resour. Conserv. Recy.*, 34 (2002) 75–90.
- [16] N. Remya, J.-G. Lin, Current status of microwave application in wastewater treatment—A review, *Chem. Eng. J.*, 166 (2011) 797–813.
- [17] G. Li, L. Wang, W. Li, Y. Xu, NiFe₂O₄/Fe₃O₄-FexNiy or FexNiy loaded porous activated carbon balls as lightweight microwave absorbents, *Rsc. Adv.*, 5 (2015) 8248–8257.
- [18] P. Hojati-Talemi, J. Azadmanjiri, G.P. Simon, A simple microwave-based method for preparation of Fe₃O₄/carbon composite nanoparticles, *Mater. Lett.*, 64 (2010) 1684–1687.
- [19] C. Namasivayam, D. Sangreetha, Recycling of agricultural solid waste, coir pith: Removal of anions, heavy metals, organics and dyes from water by adsorption onto ZnCl₂ activated coir pith carbon, *J. Hazard. Mater.*, 135 (2006) 449–452.
- [20] S.K. Theydan, M.J. Ahmed, Adsorption of methylene blue onto biomass-based activated carbon by FeCl₃ activation: Equilibrium, kinetics, and thermodynamic studies, *J. Anal. Appl. Pyrol.*, 97 (2012) 116–122.
- [21] A. Bello, O.O. Fashedemi, F. Barzegar, M.J. Madito, D.Y. Momodu, T.M. Masikhwa, J.K. Dangbegnon, N. Manyala, Microwave synthesis: Characterization and electrochemical properties of amorphous activated carbon-MnO₂ nanocomposite electrodes, *J. Alloy. Comp.*, 681 (2016) 293–300.
- [22] P. Wang, J. Mo, R. Xie, W. Jiang, Cypress sawdust based activated carbon preparation and its adsorptive capacity towards macromolecule dye (AR88): Optimization by surface methodology, *Chin. J. Environ. Eng.*, (2017) (in press).
- [23] Y. Huang, S. Li, H. Lin, J. Chen, Fabrication and characterization of mesoporous activated carbon from Lemna minor using one-step H₃PO₄ activation for Pb(II) removal, *Appl. Surf. Sci.*, 317 (2014) 422–431.
- [24] M.S. Mohy Eldin, K.M. Aly, Z.A. Khan, A.E.M. Mekky, T.S. Saleh, A.S. Al-Bogami, Removal of methylene blue from synthetic aqueous solutions with novel phosphoric acid-doped pyrazole-g-poly(glycidyl methacrylate) particles: kinetic and equilibrium studies, *Desal. Water Treat.*, 57 (2016) 27243–27258.
- [25] R. Xie, Y. Chen, T. Cheng, Y. Lai, W. Jiang, Z. Yang, Study on an effective industrial waste-based adsorbent for the adsorptive removal of phosphorus from wastewater: equilibrium and kinetics studies, *Water Sci. Technol.*, 73 (2016) 1891–1900.
- [26] E. Malkoc, Y. Nuhoglu, Determination of kinetic and equilibrium parameters of the batch adsorption of Cr(VI) onto waste acorn of *Quercus ithaburensis*, *Chem. Eng. Process.*, 46 (2007) 1020–1029.
- [27] Y. Li, X. Zhang, R. Yang, G. Li, C. Hu, The role of H₃PO₄ in the preparation of activated carbon from NaOH-treated rice husk residue, *RSC Adv.*, 5 (2015) 32626–32636.
- [28] H. Hadoun, Z. Sadaoui, N. Souami, D. Sahel, I. Toumert, Characterization of mesoporous carbon prepared from date stems by H₃PO₄ chemical activation, *Appl. Surf. Sci.*, 280 (2013) 1–7.
- [29] H. Xuan, Y. Wang, G. Lin, F. Wang, L. Zhou, X. Dong, Z. Chen, Air-assisted activation strategy for porous carbon spheres to give enhanced electrochemical performance, *RSC Adv.*, 6 (2016) 15313–15319.
- [30] L. Ling, K. Li, L. Liu, S. Miyamoto, Y. Korai, S. Kawano, I. Mochida, Removal of SO₂ over ethylene tar pitch and cellulose based activated carbon fibers, *Carbon*, 37 (1999) 499–504.
- [31] H.-T. Fang, C.-G. Liu, C. Liu, F. Li, M. Liu, H.-M. Cheng, Purification of single-wall carbon nanotubes by electrochemical oxidation, *Chem. Mater.*, 16 (2004) 5744–5750.
- [32] X. Xu, L. Xia, Q. Huang, J.D. Gu, W. Chen, Biosorption of cadmium by a metal-resistant filamentous fungus isolated from chicken manure compost, *Environ. Technol.*, 33 (2012) 1661–1670.
- [33] S. Luo, P. Qin, J. Shao, L. Peng, Q. Zeng, J.-D. Gu, Synthesis of reactive nanoscale zero valent iron using rectorite supports and its application for Orange II removal, *Chem. Eng. J.*, 223 (2013) 1–7.
- [34] C.R. Teixeira Tarley, M.A. Zezzi Arruda, Biosorption of heavy metals using rice milling by-products. Characterisation and application for removal of metals from aqueous effluents, *Chemosphere*, 54 (2004) 987–995.
- [35] K.Y. Foo, B.H. Hameed, Coconut husk derived activated carbon via microwave induced activation: Effects of activation agents, preparation parameters and adsorption performance, *Chem. Eng. J.*, 184 (2012) 57–65.
- [36] R. Han, L. Zhang, C. Song, M. Zhang, H. Zhu, L. Zhang, Characterization of modified wheat straw, kinetic and equilibrium study about copper ion and methylene blue adsorption in batch mode, *Carbohydr. Polym.*, 79 (2010) 1140–1149.
- [37] F. Marrakchi, M.J. Ahmed, W.A. Khanday, M. Asif, B.H. Hameed, Mesoporous-activated carbon prepared from chitosan flakes via single-step sodium hydroxide activation for the adsorption of methylene blue, *Int. J. Biol. Macromol.*, 98 (2017) 233–239.
- [38] V.K. Gupta, B. Gupta, A. Rastogi, S. Agarwal, A. Nayak, A comparative investigation on adsorption performances of mesoporous activated carbon prepared from waste rubber tire and activated carbon for a hazardous azo dye—Acid Blue 113, *J. Hazard. Mater.*, 186 (2011) 891–901.
- [39] X. Lu, Y. Shao, N. Gao, J. Chen, Y. Zhang, Q. Wang, Y. Lu, Adsorption and removal of clofibrate acid and diclofenac from water with MIEX resin, *Chemosphere*, 161 (2016) 400–411.
- [40] O. Hamdaoui, Batch study of liquid-phase adsorption of methylene blue using cedar sawdust and crushed brick, *J. Hazard. Mater.*, 135 (2006) 264–273.
- [41] R. Darvishi Cheshmeh Soltani, A.R. Khataee, M. Safari, S.W. Joo, Preparation of bio-silica/chitosan nanocomposite for adsorption of a textile dye in aqueous solutions, *Int. Biodeter. Biodegr.*, 85 (2013) 383–391.
- [42] T.V.N. Padmesh, K. Vijayaraghavan, G. Sekaran, M. Velan, Application of *Azolla rongpong* on biosorption of acid red 88, acid green 3, acid orange 7 and acid blue 15 from synthetic solutions, *Chem. Eng. J.*, 122 (2006) 55–63.
- [43] T.V.N. Padmesh, K. Vijayaraghavan, G. Sekaran, M. Velan, Application of two- and three-parameter isotherm models: biosorption of acid red 88 onto *Azolla microphylla*, *Bioremediat. J.*, 10 (2006) 37–44.
- [44] T. Xing, H. Kai, G. Chen, Study of adsorption and desorption performance of acid dyes on anion exchange membrane, *Color. Technol.*, 128 (2012) 295–299.
- [45] W. Konicki, D. Sibera, E. Mijowska, Z. Lendzion-Bielun, U. Narkiewicz, Equilibrium and kinetic studies on acid dye Acid Red 88 adsorption by magnetic ZnFe₂O₄ spinel ferrite nanoparticles, *J. Colloid Interface Sci.*, 398 (2013) 152–160.